Thermal fluctuations and stability of a particle levitated by a repulsive Casimir force in a liquid

Norio Inui* and Kosuke Goto
Graduate School of Engineering, University of Hyogo, Shosha 2167, Himeji, Hyogo, 671-2201, Japan
(Received 8 September 2013; published 25 November 2013)

We study the vertical Brownian motion of a gold particle levitated by a repulsive Casimir force to a silica plate immersed in bromobenzene. The time evolution of the particle distribution starting from an equilibrium position, where the Casimir force and gravitational force are balanced, is considered by solving the Langevin equation using the Monte Carlo method. When the gold particle is very close to the silica plate, the Casimir force changes from repulsive to attractive, and the particle eventually sticks to the surface. The escape rate from a metastable position is calculated by solving the Fokker-Plank equation; it agrees with the value obtained by Kramers' escape theory. The duration of levitation increases as the particle radius increases up to around 2.3 μm. As an example, we show that a 1-μm-diameter gold particle can be levitated for a significantly long time by the repulsive Casimir force at room temperature.

DOI: 10.1103/PhysRevE.88.052133 PACS number(s): 05.40.Jc, 02.50.Ey, 02.70.Bf, 68.43.−h

I. INTRODUCTION

Quantum mechanics allows an attraction between metallic plates in vacuum even if they are electrically neutral. This force, known as the Casimir force [1], arises due to the change in zero-point energy of the electromagnetic field modes [2]. The Casimir force between dielectrics depends on not only the electromagnetic properties of materials but also those of the surroundings [3]. For example, the Casimir force between a gold plate and a silica plate in vacuum is attractive for any separation distance. However, the Casimir force between a gold plate and a silica plate immersed in bromobenzene (C_6H_5Br) can be repulsive for large separation distances [4,5].

The repulsive Casimir force is expected to be useful in nanotechnology [6,7]. Particle levitation in liquid by the repulsive Casimir force, which is often known as quantum levitation, is one of the applications. Under conditions of quantum levitation, the levitated object can be smoothly rotated in a liquid. Capasso *et al*. proposed a quantum-electrodynamics device using quantum levitation [6].

The repulsive Casimir force has already been observed by researchers by atomic force microscopy (AFM), and the obtained force-distance curves agree with the theoretical values from Lifshitz's theory [8–11]. Furthermore, Munday *et al*. reported that surface-charge effects will not mask the Casimir force, and no electrostatic double-layer force is expected for clean, uncharged surfaces separated by a low-dielectric-constant fluid such as bromobenzene [4]. The essential property that causes the repulsive Casimir force between the gold and silica plates in bromobenzene is that the dielectric permittivity of bromobenzene is larger than that of silica and smaller than that of gold. These properties are satisfied in regimes below the UV. Thus, the Casimir force can be repulsive for large separations. However, the order of increasing dielectric permittivity is reversed for high-frequency regimes. Thus, above the UV, the dielectric permittivity of bromobenzene becomes smaller than that of silica, This change results in a reversal of the force from repulsive to attractive [7,12].

To deeply understand quantum levitation in liquids, we must consider thermal fluctuations. If thermal fluctuations are negligible, a levitating particle stays at an equilibrium position where the repulsive Casimir force and the gravitational force are balanced. However, the particle position in a liquid is always being changed by bombardments from surrounding molecules. Thus, a particle fluctuates about the equilibrium position. Recently, Boström *et al*. [12] found that the Casimir force changes from repulsive to attractive near the surface, and the repulsive Casimir force diverges as a particle approaches the surface. Accordingly, the above-described equilibrium position is metastable. A levitating particle escaping this metastable state eventually sticks to the surface. The duration of quantum levitation strongly depends on the particle radius. Once the particle radius decreases below a threshold, the potential barrier, which exists very close to the surface, decreases and the particle easily escapes from the metastable position. In this study, we focus on the temporal change in the probability distribution of location of a levitated particle starting from an equilibrium position along the vertical axis and consider the stability of quantum levitation, which is particularly important in terms of engineering applications.

This paper is structured as follows. In Sec. II, the potential energy of a gold particle near a silica plate in bromobenzene, which is calculated by the proximity force approximation, is expressed as a function of the separation distance between the particle and the surface. Moreover, the dependence of the equilibrium position, where the potential has a local minimum, on the particle radius is shown. In Sec. III, the temporal change in the probability distribution function of a particle starting from an equilibrium position is calculated using Monte Carlo simulation in the short-time regime. In Sec. IV, the escape rate is calculated by solving the Fokker-Planck equation and is compared with the value obtained by Kramers' escape theory. In Sec. V, we briefly mention the effect of a hindered diffusion constant of a particle near a wall on the escape rate. Finally, in Sec. VI, the Conclusion, we discuss the stability of quantum levitation and comment on several problems that should be addressed in future studies.

*inui@eng.u-hyogo.ac.jp

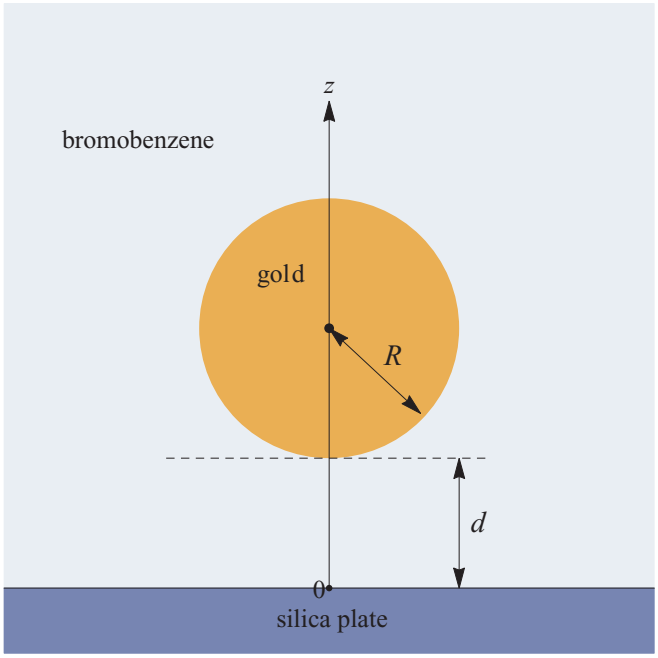

FIG. 1. (Color online) Schematic of the materials used for levitation by the repulsive Casimir force.

II. POTENTIAL ENERGY OF A LEVITATED PARTICLE

The potential energy of a gold particle of radius R placed near a silica plate in bromozenzene should be primarily considered (Fig. 1). In this section, we assume that only the Casimir force and gravitational force act on the gold particle and neglect thermal fluctuations. If the separation distance between the gold particle and the silica plate is much smaller than the particle radius, the Casimir force can be calculated using the proximity force approximation (PFA) [2]:

$$F(d) = 2\pi R E(d), \tag{1}$$

where $E(d)$ is the Casimir energy per unit area in the configuration of two parallel plates.

The Casimir energy between two plates having dielectric permittivity $\epsilon^{(1)}(\omega)$ and $\epsilon^{(2)}(\omega)$, separated by a medium having permittivity $\epsilon^{(3)}(\omega)$ at a temperature T, is given by the well-known Lifshitz formula [13]

$$E(d) = \frac{k_B T}{2\pi} {\sum_{l=0}^{\infty}}' \int_0^\infty k_\perp dk_\perp \left\{ G_{\rm TM}(\xi_l,k_\perp) + G_{\rm TE}(\xi_l,k_\perp) \right\}, \tag{2}$$

where k_B is the Boltzmann constant, and $k_\perp$ is the modulus of the wave-vector projection of light on the plate. The summation is performed over the Matsubara frequency $\xi_l = 2\pi k_B T l/\hbar$. The prime symbol near the summation sign indicates the multiplication of the term containing $l = 0$ by a factor of $1/2$. The functions $G_{\rm TM}$ and $G_{\rm TE}$ in (2) are characterized by two independent polarizations: transverse magnetic (TM) and transverse electric (TE) modes. They are defined as

$$G_{\rm TM}(\xi_l,k_\perp) = \ln\left[1 - r_{\rm TM}^{(1)} r_{\rm TM}^{(2)}(i\xi_l,k_\perp) e^{-2dk_l^{(3)}}\right],$$
$$G_{\rm TE}(\xi_l,k_\perp) = \ln\left[1 - r_{\rm TE}^{(1)} r_{\rm TE}^{(2)}(i\xi_l,k_\perp) e^{-2dk_l^{(3)}}\right],$$

where $k_l^{(n)} \equiv k_l^{(n)}(i\xi_l,k_\perp) = \sqrt{k_\perp^2 + \epsilon^{(n)}(i\xi_l)\frac{\xi_l^2}{c^2}}$. In the above equation, the reflection coefficients for the TM and TE modes are given by

$$r_{\rm TM}^{(n)}(i\xi_l,k_\perp) = \frac{\epsilon_l^{(n)} q_l - \epsilon_l^{(3)} k_l^{(n)}}{\epsilon_l^{(n)} q_l + \epsilon_l^{(3)} k_l^{(n)}}, \tag{3}$$

$$r_{\rm TE}^{(n)}(i\xi_l,k_\perp) = \frac{q_l - k_l^{(n)}}{q_l + k_l^{(n)}}, \tag{4}$$

where $\epsilon_l^n = \epsilon(i\xi_n)$. Boström *et al.* theoretically studied the Casimir force between a gold plate and a silica plate immersed in bromobenzene on the basis of the Lifshitz theory [12]. They calculated the Casimir energy from $d = 2$ nm to 2 μm and found that the sign of the Casimir force changes at approximately 3 nm. We used their results in the following calculations.

The PFA is not valid for a large separation distance between the gold particle and the silica plate [14]. Thus, we used the scattering-matrix formulation at absolute zero [15,16] for $d/R > 0.1$. In this formula, the Casimir energy is given by

$$E(d) = \frac{\hbar}{2\pi} \int_0^\infty d\xi \sum_{m=-\infty}^{\infty} \ln\det M^{(m)}. \tag{5}$$

Here, the matrix $M^{(m)}$ is given by

$$[M^{(m)}]_{ll'}^{\alpha\beta} = \delta_{ll'} - T_{lm}^{\alpha} U_{lml'm}^{\alpha\beta}, \tag{6}$$

where $\alpha,\beta \in \{\rm TM,TE\}$. In the above equation, T_{lm} and $U_{ll'}^{\alpha\beta}$ are primarily determined by Mie coefficients for the gold particle and the reflection coefficients defined in (4), respectively (for full details see Ref. [15]). To numerically evaluate the Casimir energy, the matrix $M^{(m)}$ must be truncated at a finite $l_{\rm max}$. The required value of $l_{\rm max}$ increases as d/R decreases. In contrast to the PFA, the scattering-matrix formulation gives the accurate Casimir energy for large separations. We chose $l_{\rm max} = 20$ for this study. The difference in the Casimir energy between $l_{\rm max} = 19$ and $l_{\rm max} = 20$ at $R = 500$ nm is less than 1%.

The sum of the gravitational force and buoyancy acting on the gold particle is given by

$$F_g = -\tfrac{4}{3}\pi R^3(\rho_g - \rho_b)g, \tag{7}$$

where $\rho_g = 1.932 \times 10^4$ kg/m^3 and $\rho_b = 1.489 \times 10^3$ kg/m^3 denote the mass densities of gold and bromobenzene [17], respectively, and $g = 9.8$ m/s^2 is the gravitational acceleration. As a result, the resultant force $F(d)$ acting on a gold particle of radius R is given by the sum of the Casimir force, gravitational force, and buoyancy. We define the potential energy of the gold particle as

$$\phi(d) = -\int_{d_e}^{d} F(z)dz, \tag{8}$$

where d_e is the separation distance at the equilibrium position.

Figure 2 shows the potential energy of a 500-nm-radius gold particle. A very sharp potential barrier is observed at approximately 3 nm. The inset shows the enlarged view near the surface. The separation distance at the equilibrium position is 82 nm. The absolute value of the Casimir energy

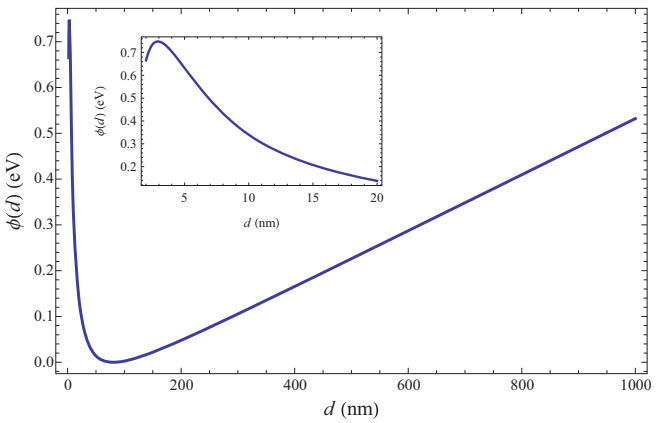

FIG. 2. (Color online) Potential energy of a 500-nm-radius gold particle as a function of separation distance between the gold particle and the silica plate.

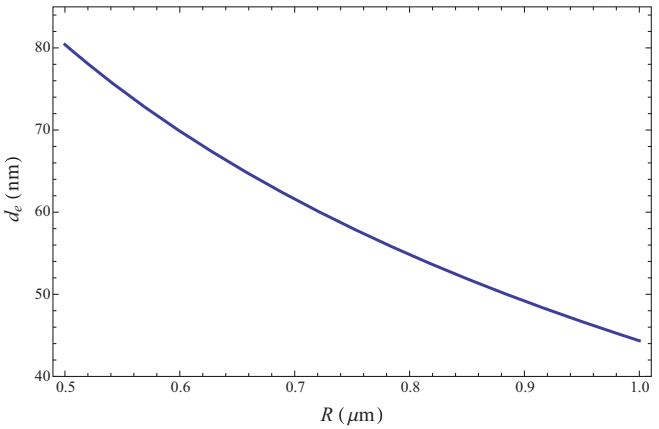

FIG. 3. (Color online) Dependence of separation distance between a gold particle and a silica plate at the equilibrium position on particle radius.

rapidly decreases as the separation distance between the gold particle and the silica plate increases for large separations. Thus, the contribution of the Casimir energy to the potential energy decreases for large separations, and the potential energy linearly increases as the separation distance increases.

The potential energy has a local maximum at approximately 3 nm; this value is rather smaller than the particle radius. Here we recall that the PFA is valid for separations much smaller than the particle radius [18]. Thus, the PFA gives a satisfactory approximation for the potential barrier height of particles larger than 3 nm in diameter. We later show that this height mainly determines the escape rate.

Figure 3 shows the levitation height of the gold particle as a function of particle radius. The Casimir force is linearly proportional to the particle radius within the PFA, given in (1), and the gravitational force is proportional to the cube of the radius. Thus, the levitation height decreases with the radius. The degree of applicability of the PFA at equilibrium is accordingly improved with the increase in radius.

III. VERTICAL PROBABILITY DISTRIBUTION FUNCTION

The most notable thermal effect on the dynamics of a levitated particle is the Brownian motion caused by random bombardments of the surrounding molecules in the liquid. The Brownian motion of a particle in an unbounded space is characterized by a diffusion constant D. In the large-time regime, the mean-squared value of the free-particle displacement that starts at time $t = 0$ from $z = z_0$ is given by

$$\langle [z(t) - z_0]^2 \rangle = 2Dt. \tag{9}$$

The diffusion constant of a particle in liquid is given by Einstein's relation [19]:

$$D = \frac{k_B T}{6\pi\eta R}, \tag{10}$$

where η is the viscosity of bromobenzene. Using the experimental data [17] $\eta = 1.080$ mPa s at 298.15 K we obtain $D = 6.36 \times 10^{-13}$ m^2/s for $R = 500$ nm.

We assume that a gold particle of mass m is initially located at the equilibrium position and consider the particle spread along the vertical axis. To obtain the probability distribution of location of a particle $P(z,t)$ at time t, we solve the Langevin equation of Ornstein-Uhlenbeck theory [20] for a position horizontal to the surface $z(t)$ and a velocity $v(t)$:

$$dz(t) = v(t)dt, \tag{11}$$

$$dv(t) = \frac{F(z(t))}{m}dt - \beta v(t)dt + dB(t), \tag{12}$$

where β is the friction coefficient per mass, and B is the Wiener process with a variance parameter $2\beta^2 D$.

The force acting on the gold particle near the equilibrium position $z_e \equiv d_e + R$ can be expressed by

$$F(z) = -k(R)(z - z_e) + O((z - z_e)^2), \tag{13}$$

where k is the effective spring constant and depends on the particle radius. For instance, k is 2.87×10^{-6} N/m for $R = 500$ nm. This spring constant is much smaller than that of a typical AFM cantilever. By linearizing the force near the equilibrium position, the Langevin equation can be exactly solved [20,21]. The evolution of the probability distribution in the short-time regime is approximately given by

$$P(z,t) \approx \left[\frac{2\pi D}{\omega^2\beta}\left\{1 - e^{-\beta t}\left(\frac{2\beta^2}{\beta_1^2}\sinh^2\frac{\beta_1 t}{2} + \frac{\beta}{\beta_1}\sinh\beta_1 t + 1\right)\right\}\right]^{-1/2} \times \exp\left[-\frac{(z - z_e)^2}{\frac{2D}{\omega^2\beta}\left\{1 - e^{-\beta t}\left(\frac{2\beta^2}{\beta_1^2}\sinh^2\frac{\beta_1 t}{2} + \frac{\beta}{\beta_1}\sinh\beta_1 t + 1\right)\right\}}\right], \tag{14}$$

where $\omega = \sqrt{k/m}$ and $\beta_1 = \sqrt{\beta^2 - 4\omega^2}$.

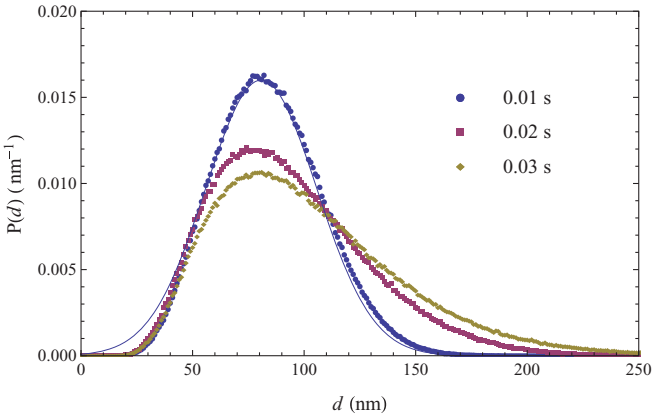

FIG. 4. (Color online) Changes in probability distributions of finding a 500-nm-radius gold particle at separation distance d. The solid line is the probability distribution function of a harmonic potential with a spring constant $k = 2.87\times10^{-6}$ N/m.

As the particle moves away from the equilibrium position, the nonlinearity of the force must be considered, and the Langevin equation cannot be solved exactly. Thus, we used the Monte Carlo method [22] to obtain the probability distribution $P(z,t)$. The Langevin equation in (12) is discretized as follows:

$$z(t+\Delta t) = z(t) + v(t)\Delta t, \tag{15}$$

$$v(t+\Delta t) = v(t) + \frac{F(z(t))}{m}\Delta t - \beta v(t)\Delta t + \Gamma, \tag{16}$$

where Γ is the external Gaussian random force with a variance $\beta\sqrt{2D\Delta t}$.

Figure 4 shows the probability distribution of a 500-nm-radius gold particle in bromobenzene that starts at $z(0) = z_e$ and $v(0) = 0$, which is obtained by accumulating 10^6 samples with $\Delta t = 59.3$ ns. Since a potential barrier exists near the surface, the distribution is asymmetric and the gold particle is more frequently found above the starting position. The solid line in Fig. 4 shows the distribution by means of the linear approximation (14) for the force at $t = 0.01$ s.

IV. ESCAPE RATE

The Casimir energy decreases without limit as the gold particle approaches a silica plate. Thus, the particle is strongly attracted to the surface and eventually sticks to it. We consider the temporal asymptotic behavior of the probability distribution after long-time-scale evolution. Since the Monte Carlo method involves significant computational complexity for long-time simulations, alternatively, we may numerically solve the Smoluchowski equation [23]. The Smoluchowski equation, a special case of the single-variable Fokker-Planck equation, describes one-dimensional Brownian motion of a particle in a force field $F(z)$ at the high-friction limit, and is given by

$$\frac{\partial P(z,t)}{\partial t} = -\frac{1}{\xi}\frac{\partial}{\partial z}[F(z)P(z,t)] + D\frac{\partial^2 P(z,t)}{\partial z^2}, \tag{17}$$

where ξ is the friction constant [20,23]. According to Stokes law [24], the friction constant can be expressed by

$$\xi = 6\pi\eta R. \tag{18}$$

Using separation of variables, we are looking for the solution of the Smoluchowski equation in the following form:

$$P(z,t) = \varphi(z)e^{-\lambda t}. \tag{19}$$

The eigenvalue λ is discretized using appropriate boundary conditions described below. Since an orthonormal basis cannot be constructed from the function $\varphi(z)$, we define the function

$$\psi_n(z) = e^{\phi(z)/2k_BT}\varphi_n(z), \tag{20}$$

where $\varphi_n(z)$ is an eigenfunction with λ_n ($n = 0,1,...$) [23]. By normalizing $\psi_n(z)$, we have an orthonormality relation:

$$\int_{z_{\min}}^{z_{\max}} \psi_n(z)\psi_m(z)dz = \delta_{nm}, \tag{21}$$

where δ_{nm} is the Kronecker symbol. The upper bound $z_{\max}$ and the lower bound $z_{\min}$ in (21) are defined below. By using the orthonormality relation, the probability distribution of the particle starting at the equilibrium position is expressed by

$$P(z,t) = e^{-\phi(z)/2k_BT}\sum_n \psi_n(z)\psi_n(z_e)e^{-\lambda_n t}. \tag{22}$$

To obtain eigenvalues and eigenfunctions of the Smoluchowski equation, we used a finite-element method, in which the space between $z_{\min}$ and $z_{\max}$ is divided into a set of small segments. We denote the width of a piece of segment j as Δ_j and the number of segments as N. The minimum of segment j is z_j, and the maximum is $z_j + \Delta_j$. We suppose that the potential in the jth segment is constant, $\phi_j \equiv \phi(z_j + \Delta_j/2)$, and the eigenfunction having the eigenvalue λ_n between z_j and $z_j + \Delta_j$ is given by

$$\psi_{j,n}(z) = A_{j,n}\cos(k_n z) + B_{j,n}\sin(k_n z), \tag{23}$$

where $k_n = \sqrt{\lambda_n/D}$ [25].

The particle experiences a strong attractive force for $d < 3$ nm. We suppose the particle to be almost completely absorbed when the separation is 2 nm or below and place an absorbing wall at $z_0 = z_{\min} \equiv 2.0$ nm $+ R$ as the boundary condition. On the other hand, since the potential energy monotonically increases above d_e, we place a reflecting wall at $z_N = z_{\max} \equiv 1.5\ \mu$m $+ R$, where the potential energy exceeds the local maximum near the surface. We observe a gap between ϕ_j and ϕ_{j+1}. Accordingly, the potential energy is discontinuous at z_{j+1}. The jump conditions for the eigenfunctions at z_{j+1} [23] are given by

$$\lim_{z\to z_{j+1}-0} e^{\phi(z)/2k_BT}\psi_{n,j}(z) = \lim_{z\to z_{j+1}+0} e^{\phi(z)/2k_BT}\psi_{n,j+1}(z), \tag{24}$$

$$\lim_{z\to z_{j+1}-0} e^{-\phi(z)/2k_BT}\psi'_{n,j}(z) = \lim_{z\to z_{j+1}+0} e^{-\phi(z)/2k_BT}\psi'_{n,j+1}(z). \tag{25}$$

These equations can be rewritten as

$$M_j(z_{j+1},k_n)\begin{bmatrix} A_{n,j} \\ B_{n,j}\end{bmatrix} = M_{j+1}(z_{j+1},k_n)\begin{bmatrix} A_{n,j+1} \\ B_{n,j+1}\end{bmatrix}. \tag{26}$$

Here the matrix $M_j(z,k_n)$ is defined by

$$M_j(z,k) = \begin{bmatrix} e^{\phi_j/2k_BT}\cos(kz) & e^{\phi_j/2k_BT}\sin(kz) \\ -ke^{-\phi_j/2k_BT}\sin(kz) & ke^{-\phi_j/2k_BT}\cos(kz) \end{bmatrix}. \tag{27}$$

The amplitudes $(A_{j+1},B_{j+1})^T$ are determined from $(A_j,B_j)^T$ as

$$\begin{bmatrix} A_{n,j+1} \\ B_{n,j+1} \end{bmatrix} = M_{j+1}^{-1}(z_{j+1},k_n)M_j(z_{j+1},k_n)\begin{bmatrix} A_{n,j} \\ B_{n,j} \end{bmatrix}. \tag{28}$$

Let us consider the characteristic equation of eigenvalues. Using the boundary condition that $\psi_n(z_0)=0$ at the absorbing wall, the amplitude $(A_{n,N-1},B_{n,N-1})^T$ is given by

$$\begin{bmatrix} A_{n,N-1} \\ B_{n,N-1} \end{bmatrix} = S(k)\begin{bmatrix} C\sin k_n z_0 \\ -C\cos k_n z_0 \end{bmatrix}, \tag{29}$$

$$S(k_n) \equiv M_{N-1}^{-1}(z_{N-1},k)M_{N-2}(z_{N-1},k) \cdots M_1^{-1}(z_1,k)M_0(z_1,k), \tag{30}$$

where C is later determined by a normalization condition. Since the boundary condition at the reflecting wall is $\psi_n'(z_N)=0$, the eigenvalue is determined as a root of the characteristic equation

$$[S_{21}(k)\sin kz_0 - S_{22}(k)\cos kz_0]\cos kz_N + [-S_{11}(k)\sin kz_0 + S_{12}(k)\cos kz_0]\sin kz_N = 0, \tag{31}$$

where $S_{ij}(k)$ denotes the element in the ith row and jth column of the matrix $S(k)$. We note that the eigenvalue is determined independently of the constant C. Finally, C is determined from the normalization condition

$$\sum_{j=0}^{N-1}\int_{z_j}^{z_{j+1}} \psi_{n,j}^2(x,k_n)dx = 1. \tag{32}$$

For $R=500$ nm, we obtain the minimum eigenvalue $\lambda_0 = 7.96\times10^{-10}\ \mathrm{s}^{-1}$ and the next minimum eigenvalue $\lambda_1 = 57.4\ \mathrm{s}^{-1}$ by numerically solving the characteristic equation (31) with $\Delta_j = 0.1$ nm for $z \leqslant 800$ nm and $\Delta_j = 10$ nm for $z > 800$ nm. The next to the minimum eigenvalue is significantly larger than the minimum eigenvalue. Thus, for large t, the asymptotic probability distribution is expressed as

$$P(z,t) \approx e^{-\phi(z)/2k_BT}\psi_0(z)\psi_0(z_e)e^{-\lambda_0 t}. \tag{33}$$

Figure 5 shows a comparison of the probability distribution obtained by the Monte Carlo simulation with the approximate probability distribution (33) at 0.1 s. Although no stationary solution exists for the Smoluchowski equation in the considered system, the eigenfunction with the minimum eigenvalue can be used to express a satisfactory approximate function of the probability distribution for the long term.

We compare the minimum eigenvalue with the escape rate given by Kramers' theory [23,26,27]:

$$r_K = \frac{D}{2\pi k_BT}\sqrt{\phi''(z_e)|\phi''(\zeta_{\max})|}e^{-\phi(\zeta_{\max})/k_BT}, \tag{34}$$

where $\zeta_{\max}$ is the position near the surface where the potential energy has a local maximum. For $R=500$ nm, we have $r_K = 9.13\times10^{-10}\ \mathrm{s}^{-1}$, which agrees well with the minimum eigenvalue $\lambda_0 = 7.96\times10^{-10}\ \mathrm{s}^{-1}$.

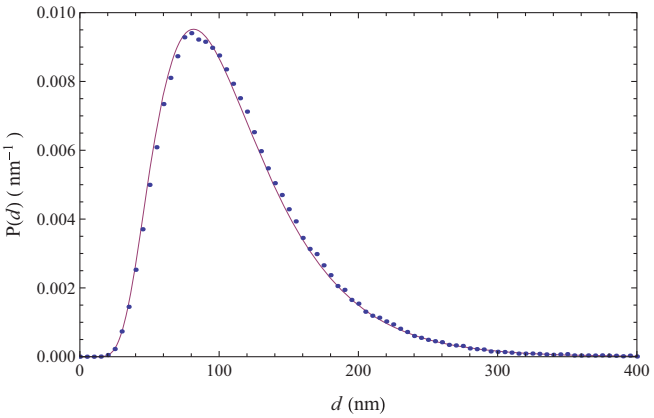

FIG. 5. (Color online) Comparison of the probability distributions at 0.1 s obtained by Monte Carlo simulation (solid circles) and the solution of the Fokker-Planck equation using the eigenfunction with the minimum eigenvalue (solid line).

We address the dependence of the duration of quantum levitation on the particle radius. According to Kramers' escape theory, the escape rate is mainly determined by the height of the potential barrier $\phi(\zeta_{\max})$. If the separation distance is much smaller than the particle radius, the Casimir energy is proportional to the particle radius. On the other hand, the gravitational potential is proportional to the cube of the particle radius. Thus, the potential barrier disappears for large particle radii. Figure 6 shows that the potential barrier height decreases above $R = 2.3\ \mu$m, which indicates a decrease in the duration of quantum levitation.

We conjecture that the duration of quantum levitation monotonically decreases below $R=500$ nm. To roughly estimate the duration of quantum levitation for submicron gold particles, we show in Fig. 7 the escape rates r_K (solid line) obtained by Kramers' theory and the minimum eigenvalues (solid circles) for $150 \leqslant R \leqslant 500$ nm. The difference between the escape rates obtained by Kramers' theory and by the minimum eigenvalues for the Smoluchowski equation increases as the radius decreases due to the decrease in the gaps between the minimum eigenvalues and others. However, both data sets suggest that the duration exponentially decreases

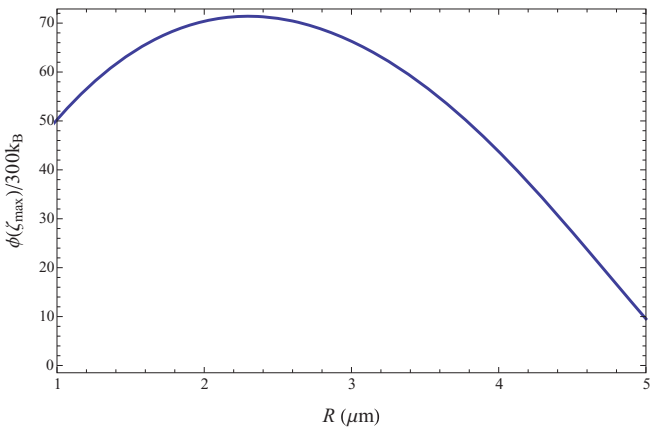

FIG. 6. (Color online) Potential barrier height near the silica surface as a function of particle radius.

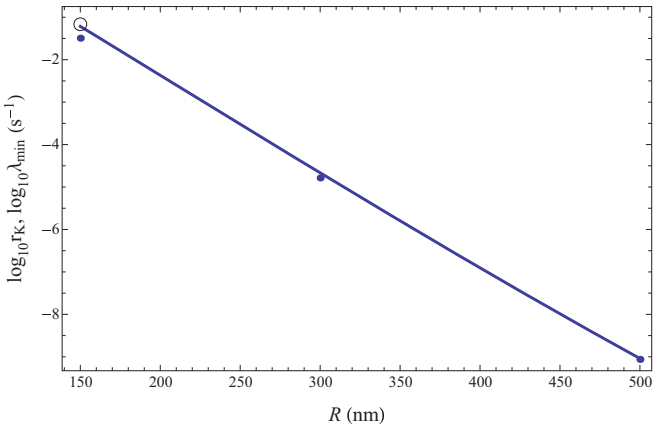

FIG. 7. (Color online) Semi-log plot of the escape rates obtained by Kramers' escape theory r_K (a solid line) and the minimum eigenvalue λ_{min} (closed circles). The open circle at $R = 150$ nm indicates a value obtained by Monte Carlo simulation.

with particle radius. The open circle in Fig. 7 is the escape rate obtained by the Monte Carlo simulation for a 150-nm-radius particle starting from the equilibrium position in which the particle is removed when the separation distance is below $d = 2$ nm. One can see good agreement between the simulated and Kramers' results. The corresponding escape rate R_K is estimated to be 0.06 s^{-1}, and the duration of quantum levitation is approximately estimated as 15 s.

V. EFFECT OF ESCAPE RATE ON HINDERED DIFFUSION

The diffusion constant of the gold particle along the vertical axis was assumed to be constant in the previous sections. However, the diffusion constant depends on the separation distance due to the hydrodynamic effect [28–30] and is expressed by

$$\frac{D(\gamma)}{D_\infty} = \frac{8 + 14\gamma + 6\gamma^2}{17 + 21\gamma + 6\gamma^2}, \tag{35}$$

where $\gamma = d/R$ and D_∞ is the diffusion constant of the unboundedly moving particle. The diffusion constant decreases as the particle approaches the surface and converges to $(8/17)D_\infty$.

Figure 8 shows the survival probability of finding a levitated particle $P_{sv}(t)$ at time t without being adsorbed on the silica plate on a semilogarithmic scale for $R = 150$ nm, which is obtained by Monte Carlo simulations. The decay of the survival probability of a particle with a hindered diffusion constant is reduced to that of a freely moving particle. Thus, the escape rate decreases when the hindered diffusion effect is considered. However, the hindered diffusion constant is limited between $(8/17)D_\infty$ and D_∞, and according to Kramers' escape theory, the correction factor to the escape rate is not below 8/17.

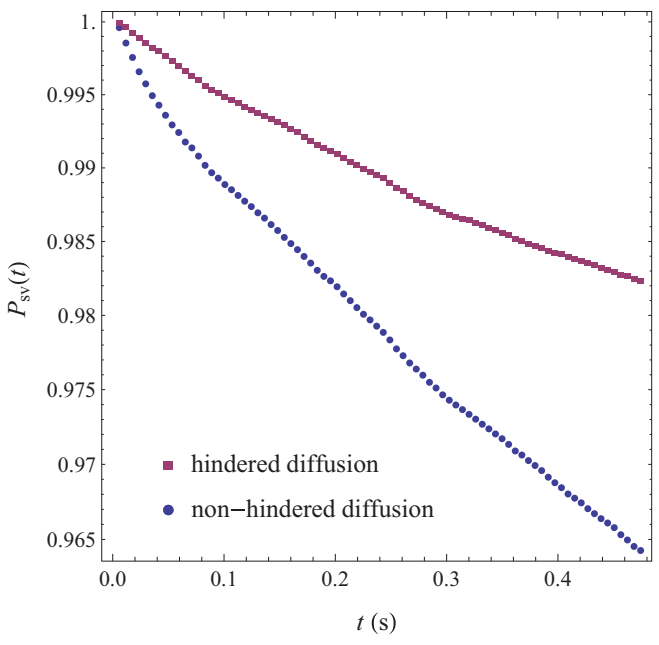

FIG. 8. (Color online) Decay of the probability of finding a levitated particle having a constant diffusion constant (closed circles) and that having a hindered diffusion constant, which depends on the position(closed squares), in a semi-log scale.

VI. CONCLUSION

In this study, we addressed the thermal effect on quantum levitation. In particular, we considered the dependence of the escape rate on particle radius by three methods: Monte Carlo simulation, solution of the Smoluchowski equation using a finite-element method, and calculation by Kramers' escape theory.

Monte Carlo simulations presented a change in the height profile caused by thermal fluctuations of a gold particle starting at an equilibrium position, which depends on the particle radius. Since a potential barrier exists near the surface, the height profile is asymmetric relative to the equilibrium position. A longer tail is observed above the equilibrium position. Collisions between a gold particle and bromobenzene molecules can cause the gold particle to escape from the equilibrium position over the potential barrier. Since a strong attractive force exists very close to the surface, the gold particle eventually sticks to it. Thus, quantum levitation does not continue always. The duration of quantum levitation strongly depends on the potential barrier near the surface.

The potential energy of the gold particle unboundedly decreases as the particle approaches the surface. Thus, a stationary height profile does not exist. To consider the asymptotic behavior of the height profile at long times, we calculated the minimum eigenvalue and its eigenfunction of the Fokker-Planck equation for Brownian motion in a nonlinear force field using a finite-element approach. The obtained eigenvalue for a 500-nm-radius gold particle was considerably smaller in comparison with the second minimum eigenvalue and the height profile of a 500-nm-gold particle can be well expressed in a practical time scale by the eigenfunction with the minimum eigenvalue. We compared the minimum eigenvalue with the value obtained by Kramers' escape theory and showed good agreement for large particle radii. The primary factor that determines the escape rate is the Boltzmann factor at the maximum of the potential barrier, which is $e^{-29} \approx 10^{-13}$ for $R = 500$ nm. The Boltzmann factor at the maximum of the potential barrier increases further as the particle radius increases up to $R = 2.4\,\mu$m, and thus the escape rate decreases.

For larger particle radii, the gravitational potential increases more rapidly than the Casimir energy and results in a decrease of the potential barrier and an increase in the escape rate.

The potential barrier decreases as the particle radius decreases below 2.3 μm. Calculations beyond the proximity approximation [15,16] should obtain accurate escape rates for smaller particle radii. However, the exponential increase in the escape rate for decreasing particle radius, which is observed in this study, would still hold. The adsorption of a levitated particle onto the surface in the short-time regime could be observed for particles below 150 nm in radius.

According to Einstein's equation for Brownian motion, the diffusion constant is proportional to the mobility, which is defined as the ratio of the velocity to the drag force. Furthermore, according to Stokes law, if a particle can freely move in a liquid, the mobility is inversely proportional to the viscosity of the liquid, independent of the position. However, in a confined system, the drag force changes near a wall depending on the distance between the moving particle and the wall. Thus, the diffusion constant also changes. The mobility decreases near a wall; this effect lengthens the duration of the quantum levitation. The lifetime of a 500-nm-radius gold particle is significantly long if hindered diffusion is not considered. Thus, we conclude that quantum levitation of a 1-μm-diameter gold particle is nearly stable with regard to its vertical axis position in practical applications. The repulsive Casimir force cannot fix a levitated particle in a plane parallel to the silica plate, and a levitated particle exhibits unbounded Brownian motion in the horizontal plane.

A well-known method to measure the height profile of Brownian motion is total internal reflection fluorescence microscopy [31]. A change in distance as small as 1 nm is detected between a sphere in an aqueous solution and a transparent plate. However, this method may not be available for the measurement of a levitated particle in bromobenzene above a silica plate because the refractive index of bromobenzene is larger than that of silica at visual frequencies. Thus, the total reflection condition is not satisfied. We must seek other methods such as confocal tracking [32] and holographic microscopy [33]. If the height profile of a levitated particle is accurately measured, the Casimir potential can also be measured. This is useful for understanding the Casimir force because the effective spring constant near equilibrium is small in comparison with a commercial AFM cantilever and high sensitivity is expected.

ACKNOWLEDGMENTS

This research was supported by the Ministry of Education, Culture, Sports, Science and Technology, a Grant-in-Aid for Scientific Research(C), MEXT KAKENHI Grant No. 25390117, and the Sanyo Special Steel Cultural Promotion Foundation.

[1] H. B. G. Casimir, Proc. Kon. Ned. Akad. Wet. B **51**, 793 (1948).
[2] M. Bordag, G. L. Klimchitskaya, U. Mohideen, and V. M. Mostepanenko, *Advances in the Casimir Effect* (Oxford University Press, New York, 2009).
[3] P. J. van Zwol, G. Palasantzas, and J. Th. M. De Hosson, Phys. Rev. B **79**, 195428 (2009).
[4] J. N. Munday, F. Capasso, and V. A. Parsegian, Nature (London) **457**, 170 (2009).
[5] M. Ishikawa, N. Inui, M. Ichikawa, and K. Miura, J. Phys. Soc. Jpn. **80**, 114601 (2011).
[6] F. Capasso, J. N. Munday, and Ho Bun Chan, in *Casimir Physics*, edited by D. Dalvit, P. Milonni, D. Roberts, and F. Rosa (Springer-Verlag, Heidelberg, 2011).
[7] A. W. Rodriguez, A. P. McCauley, D. Woolf, F. Capasso, and J. D. Joannopoulos, and S. G. Johnson, Phys. Rev. Lett. **104**, 160402 (2010).
[8] A. Milling, P. Mulvaney, and I. Larson, J. Colloid Interface Sci. **180**, 460 (1996).
[9] A. Meurk, P. F. Luckham, and L. Bergström, Langmuir **13**, 3896 (1997).
[10] S. Lee and W. M. Sigmund, J. Colloid Interface Sci. **243**, 365 (2001).
[11] R. F. Tabor, R. Manica, D. Y. C. Chan, F. Grieser, and R. R. Dagastine, Phys. Rev. Lett. **106**, 064501 (2011).
[12] M. Boström, B. E. Sernelius, I. Brevik, and B. W. Ninham, Phys. Rev. A **85**, 010701(R) (2012).
[13] E. M. Lifshitz, Soviet Phys. JETP **2**, 73 (1956).
[14] H. Gies and K. Klingmüller, Phys. Rev. Lett. **96**, 220401 (2006).
[15] P. A. Maia Neto, A. Lambrecht, and S. Reynaud, Phys. Rev. A **78**, 012115 (2008).
[16] R. Zandi, T. Emig, and U. Mohideen, Phys. Rev. B **81**, 195423 (2010).
[17] J. N. Nayak, M. I. Aralaguppi, and T. M. Aminabhavi, J. Chem. Eng. Data **48**, 628 (2003).
[18] A. Canaguier-Durand, P. A. MaiaNeto, I. Cavero-Pelaez, A. Lambrecht, and S. Reynaud, Phys. Rev. Lett. **102**, 230404 (2009).
[19] A. Einstein, Ann. Phys. (Leipzig) **17**, 549 (1905).
[20] G. E. Uhlenbeck and L. S. Ornstein, Phys. Rev. **36**, 823 (1930).
[21] E. Nelson, *Dynamical Theories of Brownian Motion* (Princeton University Press, Princeton, NJ, 2009).
[22] P. J. Rossky, J. D. Doll, and H. L. Friedman, J. Chem. Phys. **69**, 4628 (1978).
[23] H. Risken, *Fokker-Planck Equation*, Springer Series in Synergetics, Vol. 18 (Springer, Berlin, 1984).
[24] M. E. O'Neill, Mathematika **11**, 67 (1964).
[25] E. A. J. F. Peters and Th. M. A. O. M. Barenbrug, Phys. Rev. E **66**, 056702 (2002).
[26] H. A. Kramers, Physica **7**, 284 (1940).
[27] P. Hanggi, J. Stat. Phys. **42**, 105 (1986).
[28] M. A. Bevan and D. C. Prieve, J. Chem. Phys. **113**, 1228 (2000).
[29] P. Huang and K. S. Breuer, Phys. Rev. E **76**, 046307 (2007).
[30] A. Banerjee and K. D. Kihm, Phys. Rev. E **72**, 042101 (2005).
[31] D. C. Prieve, Adv. Colloid Interface Sci. **82**, 93 (1999).
[32] Hu Cang, C. M. Wong, C. S. Xu, C. Shan, A. H. Rizvi, and H. Yang, App. Phys. Lett. **88**, 223901 (2006).
[33] T. Higuchi, Q. D. Pham, S. Hasegawa, and Y. Hayasaki, Appl. Opt. **50**, H183 (2011).